HHS Public Access

Author manuscript

Ophthalmology. Author manuscript; available in PMC 2018 June 08.

Published in final edited form as:

Ophthalmology. 2017 May ; 124(5): 644–656. doi:10.1016/j.ophtha.2016.12.034.

Histology and optical coherence tomographic correlates in drusenoid pigment epithelium detachment in age-related macular degeneration

Chandrakumar Balaratnasingam, MD, PhD[1,2,3,4], **Jeffrey D. Messinger, DC**[6], **Kenneth R. Sloan, PhD**[5,6], **Lawrence A. Yannuzzi, MD**[1,2], **K. Bailey Freund, MD**[1,2,3], and **Christine A. Curcio, PhD**[6]

[1]Vitreous Retina Macula Consultants of New York, NY

[2]LuEsther T. Mertz Retinal Research Center, Manhattan Eye, Ear, and Throat Institute, New York, NY

[3]Department of Ophthalmology, New York University Langone School of Medicine, New York, NY

[4]Center for Ophthalmology and Visual Sciences, University of Western Australia, Perth, Australia

[5]Department of Computer and Information Sciences, University of Alabama at Birmingham

[6]Department of Ophthalmology, University of Alabama School of Medicine

Abstract

Purpose—Drusenoid pigment epithelium detachment (D-PED) is a known precursor to geographic atrophy in age-related macular degeneration (AMD). We sought histological correlates for spectral-domain optical coherence tomography (SD-OCT) signatures in D-PED and determined the frequency and origin of these OCT signatures in a clinical cohort of D-PED eyes.

Design—Laboratory imaging-histology comparison; Retrospective, observational cohort study.

Participants—Four donor eyes with histopathologic diagnosis of AMD (2 non-neovascular D-PED and 2 neovascular PED); 49 eyes of 33 clinic patients with non-neovascular D-PED > 2 mm in diameter.

Method—Donor eyes underwent multimodal *ex vivo* imaging including SD-OCT then processing for high-resolution histology. All clinic patients were imaged with SD-OCT, near-infrared reflectance and color photography.

Corresponding Address: Christine A. Curcio, PhD; Department of Ophthalmology; EyeSight Foundation of Alabama Vision Research Laboratories; 1670 University Boulevard Room 360; University of Alabama School of Medicine; Birmingham AL 35294-0099; Ph 205.996.8682; F 205.934.3425; curcio@uab.edu.

Disclosures: K. Bailey Freund M.D. is a consultant for Genentech, Optos, Heidelberg Engineering, Bayer HealthCare and Optovue. The other authors have no proprietary or commercial interest in any of the materials discussed in this article.

Presentations: Angiogenesis, Exudation, and Degeneration; Miami FL, February 2016. Association for Research in Vision and Ophthalmology, Seattle WA, May 2016.

Main Outcome Measures—Histologic correlates for SD-OCT signatures in D-PED; Estimate of coverage by different RPE phenotypes in the D-PED surface; Frequency and origin of histologically-verified SD-OCT signatures in a clinical cohort of D-PED eyes; Comparisons of histological features between neovascular PED and D-PED due to AMD.

Results—Intraretinal and subretinal hyperreflective foci as seen on SD-OCT correlated to RPE cells on histology. Hypertransmission of light below the RPE+basal lamina band correlated with dissociated RPE. Subretinal hyperreflective material due to acquired vitelliform lesions corresponded to regions of apically expelled RPE organelles. In the clinical cohort, all histologically verified reflectivity signatures were visible and quantifiable. The appearance of intraretinal hyperreflective foci was preceded by thickening of the RPE-basal lamina band. Compared to PEDs associated with neovascular AMD, D-PEDs had different crystallization patterns, no lipid-filled cells, and thinner basal laminar deposits.

Conclusion—Multiple RPE fates in AMD, including intraretinal cells that are highly prognostic for progression, can be reliably followed and quantified using eye-tracked serial SD-OCT. This information may be particularly useful for obtaining an accurate timeline of incipient geographic atrophy in clinic populations and for quantifying anatomic endpoints and response to therapy in AMD clinical trials.

Keywords

Retinal pigment epithelium; detachment; drusen; age-related macular degeneration; geographic atrophy; transdifferentiation; histology; spectral domain optical coherence tomography; multimodal imaging

INTRODUCTION

Age-related macular degeneration (AMD) is the leading cause of severe vision loss in older adults in the developed world. In 2014, the worldwide prevalence of AMD was estimated to be 8.7%. It is predicted that there will be 196 million people with AMD in 2020 and 288 million in 2040.[1] Geographic atrophy (GA) is an end-stage manifestation of AMD affecting >5% of European descendants over 90 years of age.[2,3] There are no proven treatments for GA although trials are in progress. A major challenge in managing GA is determining the therapeutic target(s) for halting the cascade of cellular changes that eventuates in irreversible vision loss. Clarifying the pathways leading to GA is likely to improve our ability to detect disease progression, reliably prognosticate visual outcomes, and design targeted strategies to minimize vision loss due to AMD.

Although not fully understood, the pathobiology of GA is intrinsically linked to the structure, function, and behavior of retinal pigment epithelial (RPE) cells. Drusenoid pigment epithelial detachments (D-PEDs), a hallmark feature of AMD, are a known precursor of GA.[4–7] This lesion can be distinguished from serous and hemorrhage PEDs by clinical appearance and angiography [8]. Although associated with better visual prognosis in the short-term,[8,9] the long-term prognosis of D-PED is poorer than other types of PED. The Age-related Eye Disease Study (AREDS) showed with a large sample observed for ≥ 5 years

that 19% of eyes with D-PED (defined as >350 μm diameter) progressed to central GA, 57.8% exhibited progressive fundus changes, and 39% lost >15 letters of visual acuity [10].

High-resolution optical coherence tomography (OCT) is widely used in the clinical management of AMD. In the USA alone, 4.4 million OCT scans of the macula were performed in 2012 (2012 Medicare Provider Utilization and Payment Data, https://www.cms.gov/research-statistics-data-and-systems/statistics-trends-and-reports/medicare-provider-charge-data/physician-and-other-supplier.html). OCT facilitates *in vivo* evaluation of the retina at a near-cellular level, with the axial resolution of most modern instruments corresponding to ~4μm in retinal tissue. Some of the reported precursors to collapse of D-PED and atrophy, as seen on OCT, include intraretinal hyperreflective spots, hyporeflective areas within the D-PED, subretinal hyperreflective material, and increased transmission of OCT signal into the choroid.[8,11] The cellular correspondences for these OCT signatures, if identified, may provide critical information about pathophysiologic mechanisms underlying GA.

This study utilizes high-resolution histology matched to *ex vivo* OCT B-scans from a post mortem donor eye to define a cellular basis for OCT reflectivity variations in D-PED. We build upon our recent survey of RPE phenotypes that led to a hypothesis of two major pathways of RPE fate in AMD; apoptosis and anterior migration. [12–14] The frequencies of various RPE phenotypes in D-PED are also determined using a clinical cohort of subjects imaged with spectral domain (SD) OCT. Together, histology and clinical imaging support the idea that RPE transdifferentiation to a migratory phenotype is an important antecedent of GA that can be tracked and quantified *in vivo*.

METHODS

The Institutional Review Board at UAB and the Western Institutional Review Board approved the experimental study and retrospective, observational cohort study, respectively. Research complied with the Health Insurance Portability and Accountability Act and adhered to the Tenets of the Declaration of Helsinki.

DONOR EYES, HISTOLOGY, PHOTOMICROGRAPHY AND ANALYSIS

AMD eyes were identified through an *ex vivo* imaging screen of eyes accessioned for research purposes from non-diabetic white donors to the Alabama Eye Bank during the period 1996–2012. Median death-to-preservation time was 3:49 hours (range, 0:40–11:40 hours). Eyes were preserved by immersion in 1% paraformaldehyde and 2.5% glutaraldehyde in 0.1M phosphate buffer following anterior segment excision. After vitreous removal, maculas were photographed in color on a stereomicroscope (SMZ-U, Nikon, Melville NY) [15].

Eyes underwent multimodal *ex vivo* imaging including SD-OCT when prepared for histology (2011–2013). From each globe, an 8 mm diameter full-thickness tissue punch containing the fovea and temporal portion of the optic nerve head was removed with a trephine. This punch was held in a tissue holder mounted on a Spectralis (Heidelberg Engineering, Heidelberg, Germany), as described [15]. A 30°×20° SD-OCT volume (143

scans, 30 μm spacing, automatic real time average = 25) was captured, along with red-free and near-infrared-scanning laser ophthalmoscopic images.

The left eye of a 73-year-old female donor had exceptionally clear imaging of a D-PED centered under the fovea and served as the *index* case. A macular tissue punch was postfixed by osmium tannic acid paraphenylenediamine to accentuate extracellular lipid and embedded in epoxy resin (PolyBed 812, Polysciences, Warrington PA).[16] Sub-micrometer-thick (0.8 μm) sections at 25–30 μm intervals were stained with 1% toluidine blue for polychromaticity, scanned with a 40X objective, and reviewed and photodocumented with a 60X oil-immersion objective (numerical aperture = 1.4) and digital camera (XC10, Olympus, Center Valley PA).

Diameters and heights of the D-PED central dome and surrounding drusen were measured from *ex vivo* OCT scans acquired prior to histologic processing. B-scans and subsequent histological sections were matched on the basis of overall tissue contour and patterns of distinctive reflective material. For illustration, B-scans were compressed vertically to reduce the disparity between post-mortem edema seen in the B-scan and processing-related shrinkage seen in histology. To estimate percent coverage of the D-PED by different RPE phenotypes, we recorded RPE morphology, using the terminology of Zanzottera et al [12] and Chen et al, [14] every 200 μm across each of 28 sections (total, 402 locations) using a custom Image J plug-in (http://imagej.nih.gov/ij/). Thicknesses of the RPE layer and basal laminar deposit (BLamD) were measured at the same locations. [12,13]

We compared observations from the *index* case with 3 published cases of similarly prepared PED, for a total of four post-mortem donor eyes. These included one clinically documented D-PED [17] and two clinically undocumented cases of serous and hemorrhagic PED in neovascular AMD (nvAMD). [15] New sections were obtained from prior specimens as necessary.

CLINICAL CASES AND *IN VIVO* MAGING

Clinical cases of D-PED due to non-neovascular AMD were selected retrospectively from a consecutive series of PEDs associated with AMD seen between June 2015 and January 2016 by 2 retina specialists (LY and KBF) at the Vitreous, Retina, Macula Consultants of New York, a vitreoretinal referral practice. All cases had been evaluated with color photography and fluorescein angiography and/or indocyanine green angiography using the Topcon TRC-50XF fundus camera (Topcon Medical Systems, Paramus, NJ, USA). All eyes had also been evaluated with fundus autofluorescence imaging using the Spectralis HRA + OCT (Heidelberg Engineering, Heidelberg, Germany) or the Topcon TRC-50XF fundus camera (Topcon Medical Systems, Paramus, NJ, USA)]. All eyes were also imaged with SD-OCT using the Spectralis. Eye tracking and image registration functions were enabled for all image acquisitions. The SD-OCT scan protocol is summarized in Supplementary Table 1.

Exclusion criteria were: (1) Choroidal neovascularization confirmed with SD-OCT and dye angiography. (2) Retinal artery/vein occlusion, diabetic retinopathy, previous vitreoretinal surgery, and pathologic myopia; (3) GA at the baseline clinic visit; (4) Prior ocular therapies such as laser photocoagulation or intravitreal therapy.

OCT NOMENCLATURE OF AMD PATHOLOGY

Knowledge about *ex vivo* OCT-histology correspondences derived from the *index* case and previous reports were applied to the *in vivo* OCT cohort, and the frequency of various OCT signatures was determined. Specifically, the presence or absence and frequency of OCT signatures that corresponded with intraretinal migration of RPE cells, vitelliform material, thickening of the RPE+BL band (see below), and outer retinal atrophy was determined. Regarding intraretinal hyperreflective foci we recorded the retinal layer where foci were seen and whether they formed small (1–4 foci) or large (≥5 foci) groups.

In D-PED the RPE is separated from Bruch's membrane (BrM) and also usually includes BLamD, a stereotypic thickening of the RPE basement membrane common in AMD. [12, 18–21] Therefore, we used the SD-OCT nomenclature of Staurenghi et al [22] with the substitution of RPE+BL for RPE-BrM complex.

QUANTIFYING PED MORPHOMETRY USING *IN VIVO* OCT

Morphometric characteristics of D-PEDs including volume, maximum height and maximum diameter was summarized from the clinical cohort at the clinic visit when D-PED size was judged to be the greatest. D-PED volume was determined by applying the Cavalieri principle of stereologic analysis to SD-OCT scans, [23] as we have done previously: [24,25] (i) The area between the outer boundary of the RPE+BL band and inner boundary of the BrM band for each slice in the volume was calculated using manual planimetry; (ii) The volume between two consecutive OCT slices (herein called a segment) was then determined using this equation:

$$d\left(\frac{A_x + A_{x+1}}{2}\right)$$

where:

d = distance between consecutive slices in μm.

A = Area between the RPE+BL and BrM in μm^2.

x = OCT slice number

(iii) Total D-PED volume was calculated by summing the volumes of individual segments. The number of segments in the OCT volume was (n-1) where n = total number of slices that spanned the D-PED. Maximal height (defined as the greatest distance between BrM and the outer boundary of the RPE+BL) and maximal diameter (defined as the greatest D-PED diameter along BrM) was also determined. Although the number of scans through PED varied in the clinical cohort, pilot data for our previous studies [24,25] did not demonstrate a significant difference in PED volume measurement using OCT volumes from the same eye where the distance between B-scans was 100–200 μm or 200–300 μm.

STATISTICS

Data was analyzed using descriptive statistics. Results are reported as mean ± standard deviation.

RESULTS

EX VIVO MULTIMODAL IMAGING

Ex vivo color fundus photography and near-infrared reflectance imaging of the *index* case is shown in Supplementary Figure 1. A hypopigmented lesion with pigment clumps, corresponding to the D-PED, is apparent through the thin yellow fovea. Diffuse hyperreflectivity of the central fovea and focal hyperreflectivity of surrounding lesions are seen on infrared reflectance imaging. Supplementary Video 1 is an *ex vivo* SD-OCT volume demonstrating a prominent central dome (height, 432 μm ± 33 μm) surrounded by secondary peaks. These in turn are surrounded by domes of lower elevation representing soft drusen. The base of the entire complex was 3,320 μm ± 395 μm. The base of the central dome was 1,916 μm ± 80 μm wide, i.e., ~60% of the overall width and ~36% of its area. Many reflective features are visible within the D-PED substance, on the surface, and within the overlying retina.

PED MICROSTRUCTURE

Figure 1A confirms that the PED in the *index* case is a large druse, i.e., located between BLamD and BrM. Soft drusen surrounding the central dome contained lipoprotein-derived debris and pools of lipid (Figure 1B). Subretinal drusenoid deposit, of a finer texture, filled valleys between adjacent soft drusen (Figure 1B). In the central dome (and not in the soft drusen or subretinal drusenoid deposit) were small refractile spherules known to be hydroxyapatite [26,27] and large refractile nodules (Figure 1A). Atop the dome was epithelial RPE with BLamD associated with ‘sloughed’ RPE cell bodies and ‘vitelliform’ material consisting of RPE granules mixed with outer segment debris in the subretinal space. Photoreceptors overlying the dome apex were markedly degenerated, with absent outer segments, shortened inner segments, and a thinned outer nuclear layer. Müller cells accounted for the greatest mass of retinal tissue at the point of most severe photoreceptor degeneration in the foveal center (not shown).

CORRESPONDENCES BETWEEN *EX VIVO* OCT AND HISTOLOGY

Figure 2 shows three representative pairs of matched B-scans and histology sections from the *index case*, with corresponding features indicated by color-coding. Hypertransmission (increased penetration of light below the RPE+BL band) [28] represents an atrophic area with ‘dissociated’ RPE and subsidence of the overlying outer nuclear layer (white; Figures 2A–B). Subretinal fluid was also found here (not shown). Punctate reflectivities within the D-PED represent calcium phosphate nodules (teal; Figures 2C–F). A moderate reflectivity in the subretinal space is attributable to subretinal drusenoid deposits (orange; Figures 2C–D). Simple (red; Figures 2A–B) and complex (dashed box; Figures 2C–D) groups of intraretinal hyperreflective foci represent small and large clusters of RPE cells, respectively. Clumped cell bodies within groups could not be readily separated for counting, but nuclei were discernible. The median number of nuclei in any one section was 2 (Q1, 0; Q3, 3; maximum, 7). A distinctive reflective signature reminiscent of a windswept volcanic plume (green; Figures 2E–F) represents a group of RPE cells migrating anteriorly and turning nearly 90° to track horizontally among the Henle fibers. Hyperreflective material internal to the RPE+BL

band indicates ‘vitelliform’ change (yellow, Figures 2E–F), which can include ‘sloughed’ RPE as well.

High-magnification views of RPE morphologies corresponding to hyperreflective foci found throughout the *ex vivo* SD-OCT volume are shown in Figure 3. Reference images from an age-matched eye without D-PED are also provided (Figure 3A). Figure 3B shows thin RPE (< 2 μm) in an area where the dominant RPE phenotype is ‘very nonuniform’. Figure 3C shows ‘sloughed’ RPE, i.e., a spherical and fully pigmented cell, in the subretinal space. Figures 3D–E show single pigmented ‘intraretinal’ RPE cells in the outer nuclear and ganglion cell layers, respectively. Groups of intraretinal RPE in the Henle fiber layer, including several multinucleate cells [29,30] appeared to swarm (Figure 3F). Five RPE cells were seen to form a ring around an inner retinal capillary (Figure 3G). Figure 3H shows RPE organelles in the extracellular compartment mixed with outer segment debris resulting from photoreceptor degeneration (‘vitelliform’). In an area of hypertransmission and nowhere else, the RPE layer has broken up and ‘dissociated’ RPE remain atop BLamD (Figure 3I).

Coverage of the PED surface by different RPE phenotypes is summarized in Table 1 and Supplementary Figure 2. Mean thicknesses for RPE, BLamD, and RPE+BLamD were 10.98 ± 4.63 μm, 3.95 ± 2.22 μm, and 14.93 ± 5.08 μm, respectively. At 402 assessed locations on the D-PED surface, 42 (10.4%) of the D-PED surface was associated with RPE scattered throughout layers of the overlying retina (33.3% ganglion cell layer, 7.1% inner plexiform, 11.9% inner nuclear, 7.1%–19% in synaptic and axonal portions of outer plexiform, respectively; 21.4% outer nuclear). Of locations demonstrating migrated RPE, 38.3% also demonstrated ‘vitelliform’ material. ‘Shedding’ (apoptotic) RPE was not found in any evaluated location.

COMPARISONS BETWEEN PED SUBTYPES

To determine if the *index* case was representative, it was compared to published PED cases. The first comparison case was a 41-year-old white woman who presented with a large subfoveal D-PED in 1973, documented clinically with color photography (Supplementary Figure 3A). At her death, 22 years later, *ex vivo* imaging revealed a D-PED complex (>350 μm in extent) that was unchanged in appearance since the clinic visit (Supplementary Figure 3B). Histology showed that the RPE was well pigmented, continuous, and highly variable in thickness (Supplementary Figure 3C). The D-PED had a finely granular interior with evidence of active remodeling, including cells at the superior aspect (Supplementary Figure 3D). This clinically stable D-PED had no evidence of crystallization, migrated RPE, vitelliform change, or BLamD. Instead, the RPE layer was overall thin, and the ‘shedding’ (apoptotic) RPE phenotype [12,31] predominated. Mean thicknesses for RPE, BLamD, and RPE+BLamD were 8.33 ± 5.14 μm, 0.08 ± 0.30 μm, and 8.41 ± 5.24 μm, respectively.

These D-PEDs were compared with serous and hemorrhagic PEDs reported in two eyes of two older donors with nvAMD (Table 2).[15] These PEDs had varying retinal locations (1 fovea, 1 extra-fovea), cholesterol crystals, intraretinal fluid, anteriorly migrated RPE, intraretinal lipid-filled cells, 100% coverage of the PED surface by BLamD, and no

detectable vitelliform change. Compared to PEDs associated with nvAMD, D-PEDs had different crystallization patterns, no lipid-filled cells, and thinner BLamD.

IN VIVO OCT IMAGE ANALYSIS

Of the 216 eyes with PED that were reviewed, 49 eyes of 33 patients had D-PED that met the inclusion criteria. Mean age was 74 ± 8.4 years (range 56–91 years). The cohort included 24 females, 9 males, 27 right eyes, and 22 left eyes. Mean duration of follow up was 4.9 ± 2.5 years. As measured using SD-OCT and summarized in Table 3, maximal D-PED volume, diameter, and height were 1.4 ± 1.5 mm^3, 2466.4 ± 1076.8 μm, and 344.0 ± 139.5 μm, respectively.

In vivo OCT images were evaluated for RPE and AMD changes associated with D-PED using nomenclature defined by the *index* case. An illustrative example of a 77 year-old male (similar in age to the *index* donor case) is provided in Figure 4. OCT signatures corresponding to small and large groups of intraretinal RPE cells, thickening of the RPE+BL band, loss of the ellipsoid zone at the D-PED apex, and RPE cells arranged in a ring around an inner retinal vessel were seen in the SD-OCT volume. Vitelliform material with and without ‘sloughed’ RPE cells is visible in Figure 4.

Within this cohort, hyperreflective foci were seen in 44 eyes (90%) of 29 patients. Of these, 89.4% and 42.6% of cases demonstrated foci at the level of the outer nuclear and ganglion cell layers, respectively, and 10.9% demonstrated hyperreflective foci ringed around retinal vessels. A swarm comprising 5 or more foci was seen in 70.2% of cases. Photoreceptor atrophy, characterized by loss of the ellipsoid zone and thinning of the outer nuclear layer at the D-PED apex, was seen in 45.8% of cases. It was not possible to reliably differentiate thickening of the RPE-BL band from vitelliform material in all cases. Therefore, all thickened, hyperreflective material in the subretinal space was attributed to RPE-BL thickening for analysis. It was also not possible to reliably determine RPE-BL thinning, especially in PEDs with focal areas of RPE-BL thickening. In our cohort, 35 eyes (71%) demonstrated changes corresponding to RPE-BL thickening on OCT. Evaluation of longitudinal imaging data demonstrated that intraretinal hyperreflective foci frequently appeared immediately internal to areas of RPE thickening seen in preceding visits, as demonstrated for two patients in Figure 5, strongly supporting an origin from the perturbed RPE layer below.

DISCUSSION

This study demonstrates that RPE behavior can be readily visualized *in vivo* with optimized structural SD-OCT. We defined several histology-OCT correlations in D-PED: (1) Small and large hyperreflective intraretinal foci represent fully pigmented and nucleated RPE cells that migrate anteriorly either singly or in groups; (2) Hyperreflectivity internal to the RPE-BL band resembling vitelliform lesions represent subretinal plaques of RPE organelles mixed with outer segment debris and sometimes also RPE cell bodies; (3) Hypertransmission represents dissociated RPE cells atop BLamD in an atrophic area; (4) Punctate hyperreflective foci in the D-PED interior represent refractile material among the lipid pools.

Further, in an *in vivo* cohort of D-PEDs the same size as the *index* case, 90% of eyes demonstrated OCT signatures consistent with various morphologies of intraretinal RPE.

Our *index* case supports and extends a fifty-year literature on D-PED by demonstrating contents and associated RPE changes by high-resolution epoxy-resin histology. Older papers refer to D-PED as serous or serogranular detachments, because in paraffin-based histology, D-PED had a smooth internal texture resembling fluid. Klien [32] and later S.H. Sarks [33] illustrated lesions with shortened overlying photoreceptors and intact RPE layer of non-uniform thickness. S.H. Sarks also described but did not illustrate drusen with RPE exhibiting "proliferative activity … with migration … into the retina." [34] W.R. Green and colleagues presented a large D-PED containing von Kossa-positive nodules presumed to be calcific and overlaid by subretinal and intraretinal pigmented cells [35] and a D-PED ~1 mm in diameter with partial contents and intact RPE [36]. Curcio et al illustrated the D-PED in Supplementary Figure 3. [17] Chen et al showed D-PED with hyperreflective RPE layer thickening and intraretinal foci (by *ex vivo* SD-OCT) that were ultrastructurally confirmed as RPE granules within vitelliform material and migrated cells, respectively. [14]

The *index* case provided histologic evidence for many cellular behaviors visible in both *ex vivo* and *in vivo* SD-OCT imaging. We observed solitary cells as punctate reflective foci and swarms of multiple intraretinal RPE as large irregular foci. Although most swarms comprised groups of cells, we did also note some large individual cells that were multinucleate [29,30] (Figure 5). Experimental studies in mouse demonstrated that multinucleate RPE cells in the setting of a disintegrin-like and metalloproteinase with thrombospondin type 1 motif-like 4-deficiency can be migratory [37], suggestive of a final common pathway to different stresses, while others indicate that failed cytokinesis in cell division can cause RPE multinucleation. [38] One interesting group of intraretinal RPE appeared to follow the trajectory of Henle fiber layers, resembling a previously illustrated 'plume' on SD-OCT.[14] Migrating RPE cells were seen throughout all retinal layers, even surrounding inner retinal capillaries as in bone spicule degeneration, [39] a phenomenon noted in 11% of eyes in the *in vivo* cohort. Acquired vitelliform lesions have several components, [40] and corresponding to *ex vivo* reflectivity, we found RPE granules, intact RPE cells in transit to the retina, and outer segment debris. We did not observe imaging or histological evidence of 'shaggy' (e.g., swollen) photoreceptors, [41] possibly due to the minimal subretinal fluid in this case. Finally, we showed for the first time that hypertransmission of light below the RPE-BL band, an SD-OCT sign considered diagnostic for GA,[28] can occur in an atrophic area containing 'dissociated' RPE.

We identified important differences between the *index* case and a previously published D-PED case. Numerous migrating RPE cells were seen in the *index* case (10.4% of the D-PED surface) and 'shedding' cells were rare. In contrast, in a morphologically stable DPED, the shedding RPE phenotype predominated and anteriorly migrating RPE cells and vitelliform changes were undetected, as reported elsewhere.[32, 33] Cholesterol crystallization and lipid-filled cells seen in serous and hemorrhagic PEDs were not seen in either D-PED, suggesting that these features preferentially accompany neovascularization and exudation. Thus, in this small sample, PED that progress to advanced AMD (*index* case with atrophy and the two nvAMD cases) appear to be associated with thicker BLamD and are more likely to

demonstrate hyperreflective intraretinal cells than PED that do not progress (the clinically stable case). Morphologic heterogeneity should be considered in PED-specific treatment recommendations, as reported previously, [42, 43] as PED lacking neovascularization like the *index* case may be unresponsive to VEGF suppression.

D-PED are the largest drusenoid lesions on a continuum, allowing judicious extrapolation from our data on very large D-PED to soft drusen in general. The Sarks noted that GA followed the resolution of large confluent soft drusen [5]. In the large AREDS dataset of color fundus photographs [44] Klein et al found that atrophy was preceded by a sequence of large drusen, hyper- and hypo-pigmentation, and in some instances, refractile druse contents. In 311 DPED-containing eyes from the AREDS dataset, Cukras et al concluded that large soft drusen and D-PED evolve along common pathways [10]. This commonality was reinforced by Schlanitz et al [45] who used automated OCT segmentation technology to classify >6,000 RPE elevations in patients with intermediate AMD, including ~300 D-PED by the AREDS size criterion. Ouyang et al [11] emphasized the prognostic value of hyporeflective areas appearing within drusen, the nature of which is uncertain and is a focus of our current research.

A role for intraretinal hyperreflective foci in AMD progression as seen in SD-OCT has been demonstrated with increasingly advanced imaging and analysis techniques. Discrete foci with underlying shadowing attached to RPE overlying drusen [46–49] were attributed to anteriorly migrated RPE by reference to similar foci seen in proliferative vitreoretinopathy, where RPE involvement is known. [50] Foci were also correlated with hyperpigmentation, [51,52] thus linking to knowledge of AMD progression available from population-based epidemiology [53–55]. Foci could be found as far inward as the ganglion cell layer, but more often, in photoreceptor layers [11,52]. Using eye-tracked SD-OCT to track 571 individual drusenoid lesions, Ouyang et al found that progression risk factors included large lesions, heterogeneous internal reflectivity, and presence of hyperreflective foci at baseline, with inward movement of foci over time [11] conferring the greatest risk (odds ratio, 28.2). [11] Schlanitz et al observed hyperreflective foci over 4.1% of D-PED, the highest of any lesion size class [45]. The true prognostic value of intraretinal hyperreflective foci suggested by series of very large D-PED [56] including ours will emerge from prospective studies applying objective and automated methods to a wide range of individual lesions. [45,57]

Authors of imaging studies hypothesized about the identity of hyperreflective foci related to drusen, most calling them migrated RPE [45–47, 50–52] but others also suggesting microglia pigment, macrophages with pigment inside, exudates, lipid, blood, or a degenerative retinal process conferring reflectivity.[48,58] By pairing the snapshot of histology with the movie of longitudinal clinical imaging, our study substantially narrows the window of uncertainty around intraretinal hyperreflective foci being cells of RPE origin. First, in our *index* case, all foci were found to correspond to fully pigmented cells. Second, hyperreflective foci were frequently seen to appear directly anterior to thickened RPE+BL band or vitelliform lesion on a time scale of a few months. For non-RPE cells to account for these phenomena, they would have to both match the organelle population of epithelial RPE *and* the spatiotemporal characteristics of appearing in position, precisely over and after disturbances of the layer.

An alternate hypothesis for the origin of hyperreflective foci is macrophages or microglia that ingested RPE organelles, thus taking on their reflective properties. This hypothesis is supported by experimental studies in mouse models, in which subretinal microglia are active in aging [59,60] compared to intermediate disease and worse in humans. [61, 62] Notably in human GA, pigmented cells resembling 'sloughed' and 'intraretinal' RPE express an inflammatory marker (CD163, a haptoglobin-hemoglobin scavenger) typical of bone marrow-derived macrophages, suggesting a new range of activities.[61] Transdifferentiation is the changing of a cell from one differentiated state to another. Our data support a role for transdifferentiated RPE in AMD that is unclear but can be studied by *in vivo* monitoring. These ideas about RPE are not inconsistent with well-established roles of monocyte-derived macrophages [63, 64] and inner-retina-derived microglia [61, 65] in advanced AMD. What molecular signals prompt RPE to become migratory, and whether signals arise from the sub-RPE space, neurosensory retina, or both is unspecified, although we suspect the retina due to the universally inward movement. Presumably such signals will also confront replacement cells implanted in patients with GA. [66]

Strengths of this study include the complementarity of histology and clinical SD-OCT, the use of *ex vivo* tissue imaging as a bridge to *in vivo* imaging, and a histology and photomicrography combination that provided subcellular resolution. Limitations of the histology analysis are the small number of cases overall and cases with clinical history specifically, and the lack of labeling studies to confirm cellular identities. Limitations of the *in vivo* imaging study include the unreliable differentiation of RPE-BL band thickening from vitelliform material, which may be addressable with RPE-specific detection technology, [67] and possible underestimate of mean PED height due to maximal heights falling between adjacent B-scans. Despite these shortcomings, our OCT assignments for D-PED enhance our understanding of GA pathophysiology. They also motivate new clinical studies using multimodal longitudinal imaging to determine an accurate timeline of atrophy and designing targeted therapies to mitigate this increasingly common cause of vision loss.

Supplementary Material

Refer to Web version on PubMed Central for supplementary material.

Acknowledgments

Financial support: Clinical research was supported by Macula Foundation and LuEsther T. Mertz Retinal Research Center. The Funding Organizations had no role in the design and conduct of this study. Histopathology was supported by the NIH grant R01 EY06109, and Research to Prevent Blindness, EyeSight Foundation of Alabama. Acquisition of donor eyes received additional support from International Retinal Research Foundation, National Eye Institute P30 EY003039, and the Arnold and Mabel Beckman Initiative for Macular Research. Creation of Project MACULA received additional support from the Edward N. and Della L. Thome Memorial Foundation

We thank: personnel of the Alabama Eye Bank (Doyce V. Williams, and Alan S. Blake, past and current Executive Director, respectively) for timely retrieval of donor eyes, and donor families for their gifts.

Abbreviations

AMD age-related macular degeneration

BL	basal lamina
BrM	Bruch's membrane
GA	geographic atrophy
nvAMD	neovascular AMD
PED	retinal pigment epithelium detachment
RPE	retinal pigment epithelium
SD-OCT	spectral domain optical coherence tomography

References

1. Wong WL, Su X, Li X, et al. Global prevalence of age-related macular degeneration and disease burden projection for 2020 and 2040: a systematic review and meta-analysis. Lancet Glob Health. 2014; 2(2):e106–16. [PubMed: 25104651]
2. Schmitz-Valckenberg S, Sahel JA, Danis R, et al. Natural history of geographic atrophy progression secondary to age-related macular degeneration (Geographic Atrophy Progression study). Ophthalmology. 2016; 123(2):361–8. [PubMed: 26545317]
3. Rudnicka AR, Jarrar Z, Wormald R, et al. Age and gender variations in age-related macular degeneration prevalence in populations of European ancestry: a meta-analysis. Ophthalmology. 2012; 119(3):571–80. [PubMed: 22176800]
4. Casswell AG, Kohen D, Bird AC. Retinal pigment epithelial detachments in the elderly: classification and outcome. Br J Ophthalmol. 1985; 69(6):397–403. [PubMed: 2408659]
5. Sarks JP, Sarks SH, Killingsworth MC. Evolution of geographic atrophy of the retinal pigment epithelium. Eye. 1988; 2:552–77. [PubMed: 2476333]
6. Hartnett ME, Weiter JJ, Garsd A, Jalkh AE. Classification of retinal pigment epithelial detachments associated with drusen. Graefes Arch Clin Exp Ophthalmol. 1992; 230(1):11–9. [PubMed: 1547961]
7. Roquet W, Roudot-Thoraval F, Coscas G, Soubrane G. Clinical features of drusenoid pigment epithelial detachment in age related macular degeneration. Br J Ophthalmol. 2004; 88(5):638–42. [PubMed: 15090415]
8. Mrejen S, Sarraf D, Mukkamala SK, Freund KB. Multimodal imaging of pigment epithelial detachment: a guide to evaluation. Retina. 2013; 33(9):1735–62. [PubMed: 23873168]
9. Zayit-Soudry S, Moroz I, Loewenstein A. Retinal pigment epithelial detachment. Surv Ophthalmol. 2007; 52(3):227–43. [PubMed: 17472800]
10. Cukras C, Agron E, Klein ML, et al. Natural history of drusenoid pigment epithelial detachment in age-related macular degeneration: Age-Related Eye Disease Study Report No. 28. Ophthalmology. 2010; 117(3):489–99. [PubMed: 20079925]
11. Ouyang Y, Heussen FM, Hariri A, et al. Optical coherence tomography-based observation of the natural history of drusenoid lesion in eyes with dry age-related macular degeneration. Ophthalmology. 2013; 120(12):2656–65. [PubMed: 23830761]
12. Zanzottera EC, Messinger JD, Ach T, et al. The Project MACULA retinal pigment epithelium grading system for histology and optical coherence tomography in age-related macular degeneration. Invest Ophthalmol Vis Sci. 2015; 56(5):3253–68. [PubMed: 25813989]
13. Zanzottera EC, Messinger JD, Ach T, et al. Subducted and Melanotic cells in advanced age-related macular degeneration are derived from retinal pigment epithelium. Invest Ophthalmol Vis Sci. 2015; 56(5):3269–78. [PubMed: 26024109]
14. Chen KC, Jung JJ, Curcio CA, et al. Intraretinal hyperreflective foci in acquired vitelliform lesions of the macula: clinical and histologic study. Am J Ophthalmol. 2016; 164:89–98. [PubMed: 26868959]

15. Pang C, Messinger JD, Zanzottera EC, et al. The Onion Sign in neovascular age-related macular degeneration represents cholesterol crystals. Ophthalmology. 2015; 122(11):2316–26. [PubMed: 26298717]
16. Curcio CA, Messinger JD, Mitra AM, et al. Human chorioretinal layer thicknesses measured using macula-wide high resolution histological sections. Invest Ophthalmol Vis Sci. 2011; 52(7):3943–54. [PubMed: 21421869]
17. Curcio CA, Medeiros NE, Millican CL. The Alabama Age-related Macular Degeneration Grading System for donor eyes. Invest Ophthalmol Vis Sci. 1998; 39(7):1085–96. [PubMed: 9620067]
18. Sarks SH. Ageing and degeneration in the macular region: a clinico-pathological study. Br J Ophthalmol. 1976; 60(5):324–41. [PubMed: 952802]
19. Sarks S, Cherepanoff S, Killingsworth M, Sarks J. Relationship of basal laminar deposit and membranous debris to the clinical presentation of early age-related macular degeneration. Invest Ophthalmol Vis Sci. 2007; 48(3):968–77. [PubMed: 17325134]
20. Ooto S, Vongkulsiri S, Sato T, et al. Outer retinal corrugations in age-related macular degeneration. JAMA Ophthalmol. 2014; 132(7):806–13. [PubMed: 24801396]
21. Curcio CA, Balaratnasingam C, Messinger JD, et al. Correlation of type 1 neovascularization associated with acquired vitelliform lesion in the setting of age-related macular degeneration. Am J Ophthalmol. 2015; 160(5):1024–33. e3. [PubMed: 26255578]
22. Staurenghi G, Sadda S, Chakravarthy U, Spaide RF. Proposed lexicon for anatomic landmarks in normal posterior segment spectral-domain optical coherence tomography: The IN*OCT Consensus. Ophthalmology. 2014; 121(8):1572–8. [PubMed: 24755005]
23. Prakash YS, Smithson KG, Sieck GC. Application of the Cavalieri principle in volume estimation using laser confocal microscopy. Neuroimage. 1994; 1(4):325–33. [PubMed: 9343582]
24. Balaratnasingam C, Hoang QV, Inoue M, et al. Clinical characteristics, choroidal neovascularization and predictors of visual outcomes in acquired vitelliform lesions. Am J Ophthalmol. 2016 Sep 15. 16 online.
25. Balaratnasingam C, Yannuzzi LA, Querques G, et al. Associations between retinal pigment epithelium and drusen volume changes during the lifecycle of large drusenoid pigment epithelial detachments. Invest Ophthalmol Vis Sci. 2016 Sep 4. 16 accepted.
26. Suzuki M, Curcio CA, Mullins RF, Spaide RF. Refractile drusen: clinical imaging and candidate histology. Retina. 2015; 35(5):859–65. [PubMed: 25768253]
27. Thompson RB, Reffatto V, Bundy JG, et al. Identification of hydroxyapatite spherules provides new insight into subretinal pigment epithelial deposit formation in the aging eye. Proc Natl Acad Sci U S A. 2015; 112(5):1565–70. [PubMed: 25605911]
28. Schaal KB, Rosenfeld PJ, Gregori G, et al. Anatomic clinical trial endpoints for nonexudative age-related macular degeneration. Ophthalmology. 2016; 123(5):1060–79. [PubMed: 26952592]
29. Ach T, Huisingh C, McGwin G Jr, et al. Quantitative autofluorescence and cell density maps of the human retinal pigment epithelium. Invest Ophthalmol Vis Sci. 2014; 55(8):4832–41. [PubMed: 25034602]
30. Starnes AC, Huisingh C, McGwin G, et al. Multi-nucleate retinal pigment epithelium cells of the human macula exhibit a characteristic and highly specific distribution. Vis Neurosci. 2016; 33:E001. [PubMed: 26923500]
31. Ach T, Tolstik E, Messinger JD, et al. Lipofuscin re-distribution and loss accompanied by cytoskeletal stress in retinal pigment epithelium of eyes with age-related macular degeneration. Invest Ophthalmol Vis Sci. 2015; 56(5):3242–52. [PubMed: 25758814]
32. Klien BA. The heredodegeneration of the macula lutea: diagnostic and differential diagnostic considerations and a histopathologic report. Am J Ophthalmol. 1950; 33(3–1):371–9.
33. Sarks SH. Council Lecture: Drusen and their relationship to senile macular degeneration. Aust J Ophthalmol. 1980; 8(2):117–30. [PubMed: 6160841]
34. Sarks SH, van Driel D, Maxwell L, Killingsworth M. Softening of drusen and subretinal neovascularization. Trans Ophthalmol Soc U K. 1980; 100(3):414–22. [PubMed: 6171074]
35. Green WR, Key SN 3rd. Senile macular degeneration: a histopathologic study. Trans Am Ophthalmol Soc. 1977; 75:180–254. [PubMed: 613523]

36. Bressler NM, Silva JC, Bressler SB, et al. Clinicopathological correlation of drusen and retinal pigment epithelial abnormalities in age-related macular degeneration. Retina. 1994; 14(2):130–42. [PubMed: 8036323]
37. Collin GB, Hubmacher D, Charette JR, et al. Disruption of murine Adamtsl4 results in zonular fiber detachment from the lens and in retinal pigment epithelium dedifferentiation. Hum Mol Genet. 2015; 24(24):6958–74. [PubMed: 26405179]
38. Chen M, Rajapakse D, Fraczek M, et al. Retinal pigment epithelial cell multinucleation in the aging eye - a mechanism to repair damage and maintain homoeostasis. Aging Cell. 2016; 15(3): 436–45. [PubMed: 26875723]
39. Li Z-Y, Possin DE, Milam AH. Histopathology of bone spicule pigmentation in retinitis pigmentosa. Ophthalmology. 1995; 102(5):805–16. [PubMed: 7777280]
40. Freund KB, Laud K, Lima LH, et al. Acquired vitelliform lesions: correlation of clinical findings and multiple imaging analyses. Retina. 2011; 31(1):13–25. [PubMed: 21102371]
41. Shields CL, Kaliki S, Rojanaporn D, et al. Enhanced depth imaging optical coherence tomography of small choroidal melanoma: comparison with choroidal nevus. Archives of Ophthalmology. 2012; 130(7):850–6. [PubMed: 22776921]
42. Ritter M, Bolz M, Sacu S, et al. Effect of intravitreal ranibizumab in avascular pigment epithelial detachment. Eye (Lond). 2010; 24(6):962–8. [PubMed: 19911018]
43. Arora S, McKibbin M. One-year outcome after intravitreal ranibizumab for large, serous pigment epithelial detachment secondary to age-related macular degeneration. Eye (Lond). 2011; 25(8): 1034–8. [PubMed: 21597485]
44. Klein ML, Ferris FL 3rd, Armstrong J, et al. Retinal precursors and the development of geographic atrophy in age-related macular degeneration. Ophthalmology. 2008; 115(6):1026–31. [PubMed: 17981333]
45. Schlanitz FG, Sacu S, Baumann B, et al. Identification of drusen characteristics in age-related macular degeneration by polarization-sensitive optical coherence tomography. Am J Ophthalmol. 2015; 160(2):335–44. e1. [PubMed: 25982973]
46. Pieroni CG, Witkin AJ, Ko TH, et al. Ultrahigh resolution optical coherence tomography in non-exudative age related macular degeneration. Br J Ophthalmol. 2006; 90(2):191–7. [PubMed: 16424532]
47. Fleckenstein M, Charbel Issa P, Helb HM, et al. High-resolution spectral domain-OCT imaging in geographic atrophy associated with age-related macular degeneration. Invest Ophthalmol Vis Sci. 2008; 49(9):4137–44. [PubMed: 18487363]
48. Schuman SG, Koreishi AF, Farsiu S, et al. Photoreceptor layer thinning over drusen in eyes with age-related macular degeneration imaged in vivo with spectral-domain optical coherence tomography. Ophthalmology. 2009; 116(3):488–96. e2. [PubMed: 19167082]
49. Keane PA, Patel PJ, Liakopoulos S, et al. Evaluation of age-related macular degeneration with optical coherence tomography. Surv Ophthalmol. 2012; 57(5):389–414. [PubMed: 22898648]
50. Zacks DN, Johnson MW. Transretinal pigment migration: an optical coherence tomographic study. Arch Ophthalmol. 2004; 122(3):406–8. [PubMed: 15006864]
51. Ho J, Witkin AJ, Liu J, et al. Documentation of intraretinal retinal pigment epithelium migration via high-speed ultrahigh-resolution optical coherence tomography. Ophthalmology. 2011
52. Folgar FA, Chow JH, Farsiu S, et al. Spatial correlation between hyperpigmentary changes on color fundus photography and hyperreflective foci on SDOCT in intermediate AMD. Investigative Ophthalmology & Visual Science. 2012; 53(8):4626–33. [PubMed: 22589439]
53. Klein R, Klein BE, Tomany SC, et al. Ten-year incidence and progression of age-related maculopathy: The Beaver Dam eye study. Ophthalmology. 2002; 109(10):1767–79. [PubMed: 12359593]
54. Klein R, Klein BE, Knudtson MD, et al. Fifteen-year cumulative incidence of age-related macular degeneration: the Beaver Dam Eye Study. Ophthalmology. 2007; 114(2):253–62. [PubMed: 17270675]
55. Joachim ND, Mitchell P, Kifley A, Wang JJ. Incidence, progression, and associated risk factors of medium drusen in age-related macular degeneration: findings from the 15-year follow-up of an Australian cohort. JAMA Ophthalmol. 2015

56. Clemens CR, Alten F, Heiduschka P, Eter N. Morphology score as a marker of retinal function in drusenoid pigment epithelial detachment. Retina. 2015; 35(7):1351–9. [PubMed: 25658174]
57. Schlanitz FG, Baumann B, Kundi M, et al. Drusen volume development over time and its relevance to the course of age-related macular degeneration. Br J Ophthalmol. 2016
58. Christenbury JG, Folgar FA, O'Connell RV, et al. Progression of intermediate age-related macular degeneration with proliferation and inner retinal migration of hyperreflective foci. Ophthalmology. 2013; 120(5):1038–45. [PubMed: 23352193]
59. Xu H, Chen M, Manivannan A, et al. Age-dependent accumulation of lipofuscin in perivascular and subretinal microglia in experimental mice. Aging Cell. 2008; 7(1):58–68. [PubMed: 17988243]
60. Xu H, Chen M, Forrester JV. Para-inflammation in the aging retina. Prog Retin Eye Res. 2009; 28(5):348–68. [PubMed: 19560552]
61. Lad EM, Cousins SW, Van Arnam JS, Proia AD. Abundance of infiltrating CD163+ cells in the retina of postmortem eyes with dry and neovascular age-related macular degeneration. Graefes Arch Clin Exp Ophthalmol. 2015; 253(11):1941–5. [PubMed: 26148801]
62. Greferath U, Guymer RH, Vessey KA, et al. Correlation of histologic features with in vivo imaging of reticular pseudodrusen. Ophthalmology. 2016; 123(6):1320–31. [PubMed: 27039021]
63. Sarks JP, Sarks SH, Killingsworth MC. Morphology of early choroidal neovascularization in age-related macular degeneration: correlation with activity. Eye. 1997; 11:515–22. [PubMed: 9425418]
64. Grossniklaus HE, Cingle KA, Yoon YD, et al. Correlation of histologic 2-dimensional reconstruction and confocal scanning laser microscopic imaging of choroidal neovascularization in eyes with age-related maculopathy. Arch Ophthalmol. 2000; 118:625–9. [PubMed: 10815153]
65. Gupta N, Brown KE, Milam AH. Activated microglia in human retinitis pigmentosa, late-onset retinal degeneration, and age-related macular degeneration. Exp Eye Res. 2003; 76(4):463–71. [PubMed: 12634111]
66. Nazari H, Zhang L, Zhu D, et al. Stem cell based therapies for age-related macular degeneration: The promises and the challenges. Prog Retin Eye Res. 2015; 48:1–39. [PubMed: 26113213]
67. Schütze C, Wedl M, Baumann B, et al. Progression of retinal pigment epithelial atrophy in antiangiogenic therapy of neovascular age-related macular degeneration. Am J Ophthalmol. 2015; 159(6):1100–14. e1. [PubMed: 25769245]

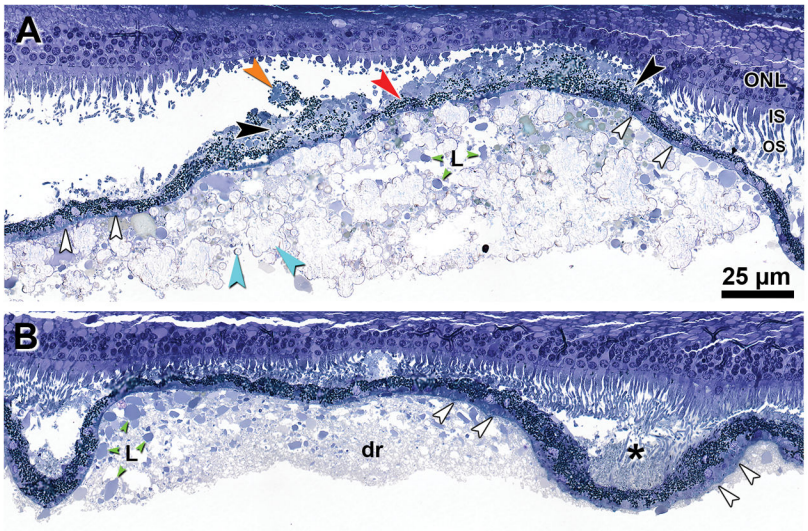

Figure 1. Microstructure and cellular associations of drusenoid pigment epithelium detachment in the *Index* case

Sections were acquired between scans 19 and 27 as shown on Supplementary Figure 1B. **A.** Central dome is comprised of mixed lipid pools (L, green) and small refractile spherules of calcium phosphate (hydroxyapatite) and large refractile nodules (teal). The RPE layer is intact but is thin and irregular (red) with a thin layer of basal laminar deposit (white). 'Sloughed' RPE (orange) and 'vitelliform' lesions (black) are also seen in the subretinal space. At the apex of the PED is prominent photoreceptor degeneration (absent OS, very short IS, thinned ONL). **B.** Soft druse (dr) contains lipoprotein-derived debris (appearing granular at this magnification) and lipid pools (L, green). Subretinal drusenoid deposit (asterisk) has a finer texture than the druse. ONL = outer nuclear layer; IS = inner segments; L = lipid pools; OS = outer segments. Scale bar in **A** applies to both panels.

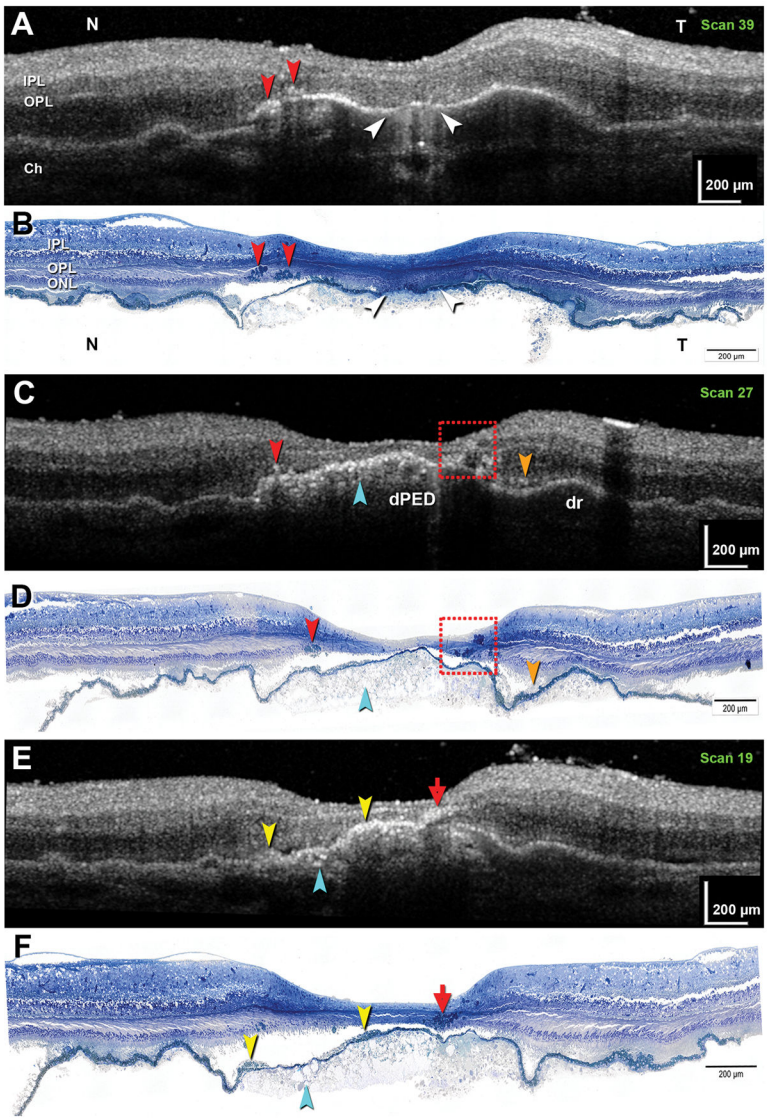

Figure 2. Correlations between *ex vivo* spectral domain optical coherence tomography and high-resolution histology in drusenoid pigment epithelium detachment in the *Index* case

Matched histology-OCT pairs taken from indicated scan levels of Supplementary Figure 1 are presented (A–B, C–D, E–F, respectively). **A,B:** Hypertransmission is associated with atrophy and 'dissociated' RPE (white arrowhead). Two groups of RPE cells are apparent (red arrowhead). **C,D:** A small cluster (red arrowhead) and multiple clusters (red dashed box) of RPE are apparent. Calcium phosphate nodules are hyperreflective (teal arrowhead). Subretinal drusenoid deposits are moderately reflective (orange). **E,F:** An 'RPE plume' is created by a group of RPE cells tracking among the Henle fibers (red arrow). Hyperreflective material internal to the RPE+BL band represents a 'vitelliform' lesion (yellow arrowheads). Calcium phosphate nodules are present (teal arrowhead). IPL, inner plexiform layer; OPL, outer plexiform layer; ONL, outer nuclear layer; Ch, choroid.

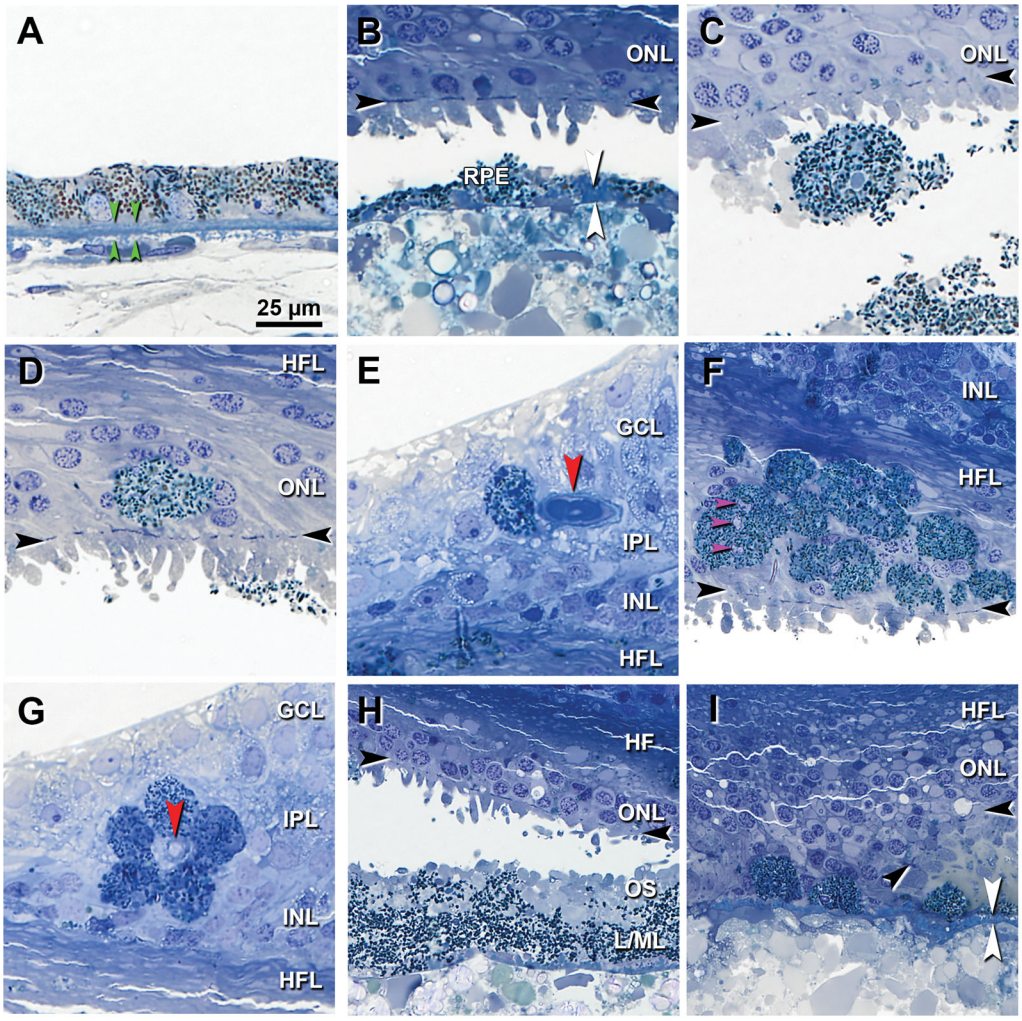

Figure 3. Histological correlates of hyperreflective structures seen in *ex vivo* optical coherence tomography of *Index* case

Panels indicate representative examples matched to reflectivities in the *ex vivo* SD-OCT volume scan. Black arrowheads, external limiting membrane, if present. GCL = ganglion cell layer; IPL = inner plexiform layer; INL = inner nuclear layer; HFL = Henle fiber layer. Scale bar in A applies to all. **A.** Nonuniform RPE. Green arrowheads, BrM. **B.** Thin, 'very non-uniform' RPE with basal laminar deposit (white arrowheads). **C.** Fully pigmented 'sloughed' RPE in the subretinal space. **D.** Fully pigmented 'intraretinal' RPE in the ONL (D). **E.** Nucleated RPE in the GCL. **F.** A swarm of 'intraretinal' RPE. One cell has 3 nuclei (pink arrowheads). **G.** Five RPE cells surround a vessel in the superficial capillary plexus. **H. '**Vitelliform' change, characterized by exploded RPE lipofuscin/melanolipofuscin granules (L/ML), outer segment (OS) debris resulting from photoreceptor degeneration, and intact RPE (not shown here). **I.** In an atrophic area individual 'dissociated' RPE cells sit atop basal laminar deposit (white). At the edge of atrophy the external limiting membrane (black arrowheads) is curved as it descends to BrM.

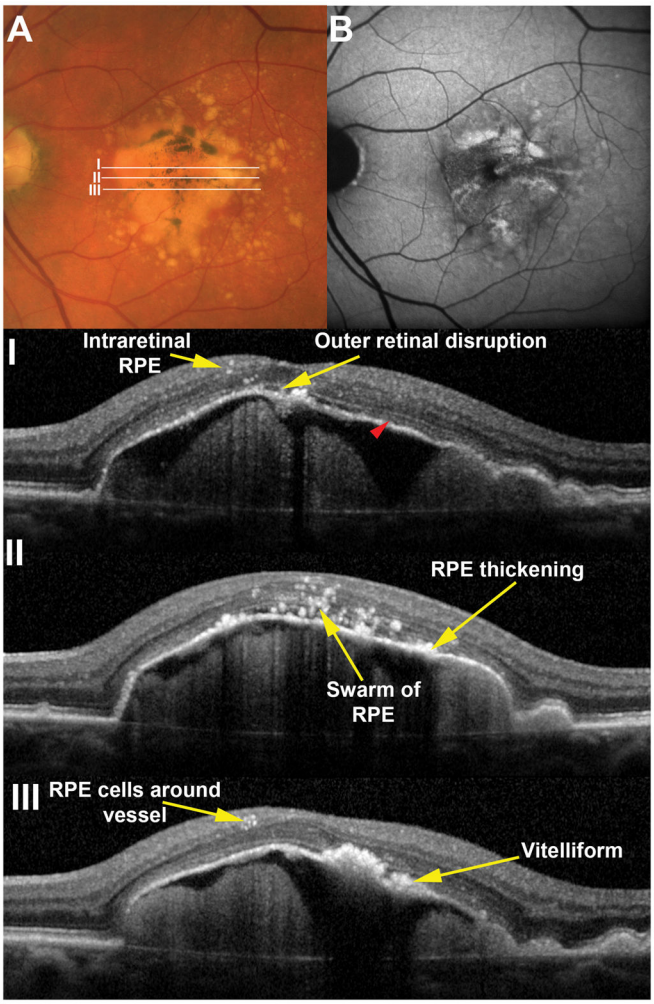

Figure 4. Histologically defined features are visible in vivo

A large drusenoid pigment epithelial detachment (D-PED) in a 77 year-old male demonstrates pigmentary changes on the surface that correlate to sites of increased fundus autofluorescence (B). Areas of B-scans (I, II and III) are illustrated in the color image. A range of RPE related changes are seen in OCT scans including intraretinal RPE cells and vitelliform lesions. Note that the ellipsoid zone (red arrowhead) is visible on the surface of the PED with the exception of the apex where it is notably absent. In this case it was possible to distinguish vitelliform lesions from RPE thickening however this distinction was not possible in most cases in this series.

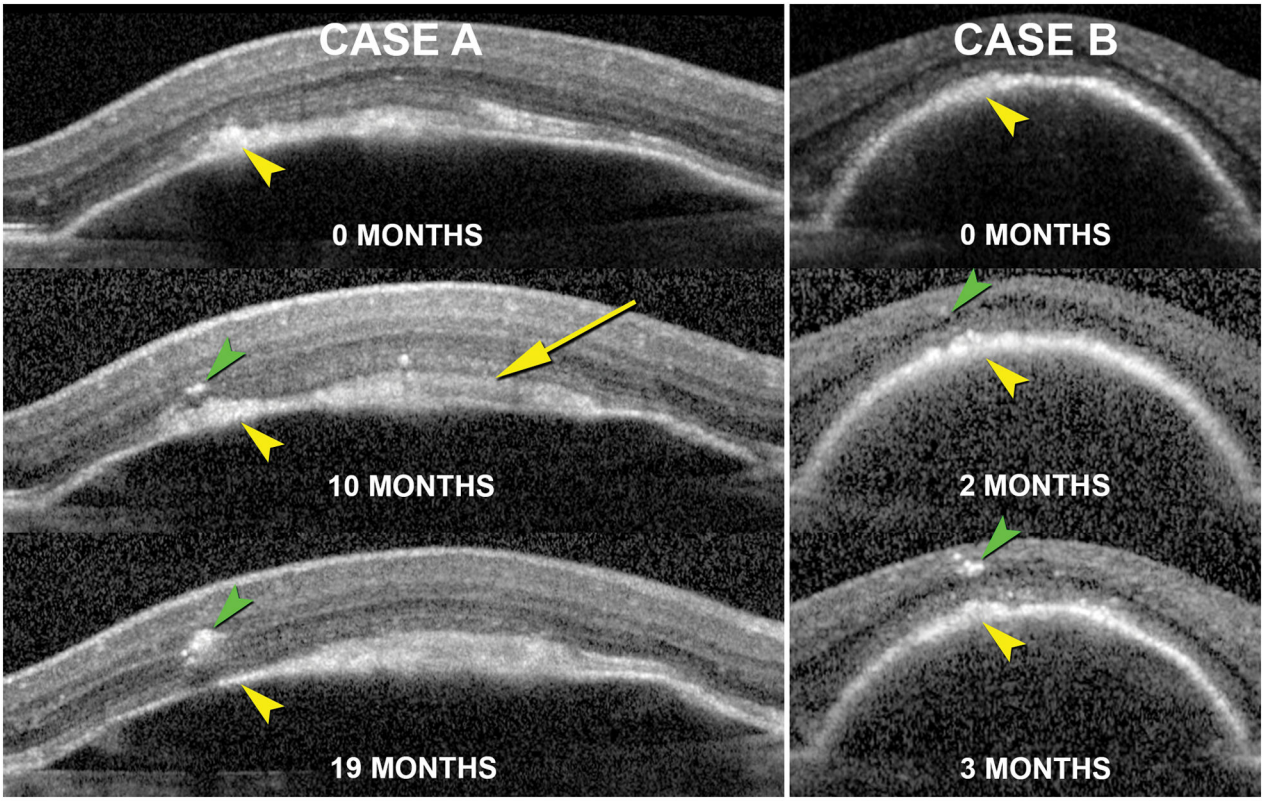

Figure 5. Association of intraretinal hyperreflective foci and thickening of the RPE+BL band during the lifecycle of drusenoid PEDs (D-PED)

The natural course of D-PED of a 71 year-old female (Case A) and 68 year-old female (Case B) as seen using in vivo SD-OCT with image registration enabled are presented. At their first visit (0 months) hyperreflective material is seen at the level of the RPE and subretinal space (yellow arrows) in both cases. Over the course of time, hyperreflective foci are seen to migrate from the RPE+BL band into the retina (green arrowheads). The rate of RPE migration and the quantity of cells migrating into the retina were different in the two cases. Yellow arrowheads denote the same location in the PED in image-registered sections and may signify vitelliform material in addition to RPE cell bodies in transit. White arrow (Case A, 10 month) also shows vitelliform material.

Table 1

Frequencies of RPE phenotypes in drusenoid pigment epithelial detachment

RPE morphology*	Locations at each grade		Associated with migrated RPE		Not associated with migrated RPE	
Not gradable	2	0.5%	0	0.0%	2	0.5%
Uniform	22	5.5%	0	0.0%	22	5.5%
Non-Uniform	237	59.0%	2	0.5%	235	58.5%
Very Non-Uniform	49	12.2%	4	1.0%	45	11.2%
Sloughing	16	4.0%	1	0.2%	15	3.7%
Shedding	10	2.5%	0	0.0%	10	2.5%
Vacuolated	2	0.5%	0	0.0%	2	0.5%
Intraretinal **	15	3.7%	--	--	--	--
Vitelliform	47	11.7%	18	4.5%	29	7.2%
Atrophy with BLamD	1	0.2%	1	0.2%	0	0.0%
Dissociated	1	0.2%	1	0.2%	0	0.0%
Atrophy without BLamD	0	0.0%	0	0.0%	0	0.0%
Total	**402**	**100.0%**	**42**	**10.4%**	**360**	**89.6%**

*Phenotypes were originally assigned per Zanzottera et al [12]. Vitelliform was demonstrated by Chen et al [14] and signifies RPE organelles exploded into the extracellular space, possibly accompanied by intact RPE cell bodies.

**The Intraretinal morphology is, by definition, migrated RPE. BLamD, basal laminar deposit

Table 2

comparison of four pigment epithelium detachments in age-related macular degeneration, characterized with *ex vivo* imaging and high-resolution histology

	Index Case	ALARMGS*	Onion 1**	Onion 2**
AMD diagnosis	**Nonneovascular**	**Nonneovascular, clinically stable**	**Neovascular**	**Neovascular**
Age, sex	73, F	63, F	98, F	91, M
PED type	Drusenoid	Drusenoid	Hemorrhagic	Serous
PED location	Fovea	Fovea	Fovea	Extra-fovea
Crystalline content	Hydroxyapatite	None	Cholesterol	Cholesterol
Intraretinal fluid	No	No	Yes	Yes
Anteriorly migrated RPE	Yes	No	Yes	Yes
Vitelliform RPE	Yes	No	No	No
Intraretinal lipidfilled cells	No	No	Yes	Yes
# Assessment locations	402	14	4	15
% Assessment locations with BLamD	93.3%	7.1%	100.0%	100.0%
Mean RPE thickness	10.98 ± 4.63	8.33 ± 5.14	10.77 ± 3.87	8.62 ± 4.88
Mean BLamD thickness	3.95 ± 2.22	0.08 ± 0.30	11.88 ± 9.82	9.77 ± 4.01
Mean RPE+BLamD thickness	14.93 ± 5.08	8.41 ± 5.24	22.65 ± 7.12	18.39 ± 5.05

Notes:

Originally published * [17]; ** [21]

Onion 2 had 6 PEDs with SD-OCT Onion Sign; all were extra-foveal.

Table 3

Summary of morphometric characteristics of 49 cases of drusenoid PED from the *in vivo* OCT cohort

	Mean ± SD	Median	Minimum	Maximum
PED Diameter (μm)	2466.4 ± 1076.8	2295	904	5072
PED Height (μm)	344.0 ± 139.5	335.5	164	659
PED Volume (mm^3)	1.4 ± 1.5	1.1	0.1	5.8